

Graphical Abstract

Adaptable and Interpretable Framework for Anomaly Detection in Streaming Energy Systems

Marek Wadinger, Michal Kvasnica

Highlights

Adaptable and Interpretable Framework for Anomaly Detection in Streaming Energy Systems

Marek Wadinger, Michal Kvasnica

- Combines interpretability with adaptation to change points in single anomaly detection system
- Isolates root cause of anomalies considering relationships between features
- Demonstrates interpretability by providing process limits for each feature
- Demonstrates comparable detection accuracy to established general methods

Adaptable and Interpretable Framework for Anomaly Detection in Streaming Energy Systems

Marek Wadinger^{a,*}, Michal Kvasnica^a

^a*Institute of Information Engineering, Automation and Mathematics, Slovak University of Technology in Bratislava, Radlinskeho 9, Bratislava, 812 37, Bratislava, Slovakia*

Abstract

In this paper, we introduce an Adaptable and Interpretable Framework for Anomaly Detection (AID) designed for streaming energy systems utilizing IoT devices. AID leverages adaptive conditional probability distribution modeling to capture the normal operation of dynamic systems and isolate root causes of anomalies. The framework dynamically updates parameter of multivariate Gaussian distribution, allowing it to adapt to non-stationarity. AID interprets anomalies as significant deviations from conditional probability, encompassing interactions as well as both spatial and temporal irregularities by exposing them as features. Additionally, dynamic process limits are drawn to pinpoint root causes. The framework also alerts individual signal as outliers in sampling. Two real-world case studies showcase AID's capabilities. The first study focuses on Battery Energy Storage Systems (BESS), demonstrating AID's effectiveness in capturing system anomalies, providing less conservative signal limits, and leveraging a physical model for temperature anomaly detection. The second case study delves into monitoring temperature profiles of battery modules, where AID successfully identifies hardware faults, emphasizing its importance in energy storage system safety and profitability. A benchmark evaluation on industrial data shows that AID delivers comparable results to other self-learning adaptable anomaly detection methods, with the added advantage of root cause isolation.

Keywords: Anomaly detection, Root cause isolation, Iterative learning control, Statistical learning, IoT

*

Email address: marek.wadinger@stuba.sk (Marek Wadinger)
URL: uiam.sk/~wadinger (Marek Wadinger)

¹ 1. Introduction

² Anomaly detection systems play a critical role in risk-averse systems by
³ identifying abnormal patterns and adapting to novel expected patterns in
⁴ data. These systems are particularly vital in the context of Internet of Things
⁵ (IoT) devices that continuously stream high-fidelity data to control units.

⁶ In this rapidly evolving field, Chandola et al. conducted an influential
⁷ review of prior research efforts across diverse application domains Chandola
⁸ et al. (2009). Recent studies have underscored the need for holistic and tun-
⁹ able anomaly detection methods accessible to operators(Laptev et al. (2015);
¹⁰ Kejariwal (2015); Cook et al. (2020)).

¹¹ Cook et al. denote substantial aspects that pose challenges to anomaly
¹² detection on IoT, including the temporal, spatial, and external context of
¹³ measurements, multivariate characteristics, noise, and nonstationarity (Cook
¹⁴ et al. (2020)). Feature engineering methods allow the encoding of contextual
¹⁵ properties and enhance the performance (Fan et al. (2019)). However, ex-
¹⁶ tensive feature engineering may significantly increase dimensionality, requir-
¹⁷ ing sizeable data storage and high computational resources (Talagala et al.
¹⁸ (2021)).

¹⁹ Moreover, nonstationarity resulting from concept drift, an alternation in
²⁰ the pattern of data due to a change in statistical distribution, and change
²¹ points, permanent changes to the system’s state, represents a difficulty of a
²² significant extent (Salehi and Rashidi (2018)). In real-world scenarios, those
²³ changes are frequently unpredictable in their spatial and temporal character-
²⁴ istics and require systems with solid outlier rejection properties of intelligent
²⁵ tracking algorithms (Barbosa Roa et al. (2019)). Therefore, the ability of an
²⁶ anomaly detection method to adapt to changes in the data structure is cru-
²⁷ cial for long-term deployments. Nevertheless, as (Tartakovsky et al. (2013))
²⁸ remarked, instantaneous detection is not an option, unless the false alarm
²⁹ risk is high

³⁰ The former scalability problem now introduces a significant latency in de-
³¹ tector adaptation (Wu et al. (2021)). Incremental learning methods allowed
³² adaptation while restraining the storage of the whole dataset. The supervised
³³ operator-in-the-loop solution offered by Pannu et al. showed the detector’s
³⁴ adaptation to data labeled on the flight (Pannu et al. (2012)). Others ap-
³⁵ proached the problem as sequential processing of bounded data buffers in

36 univariate signals (Ahmad et al. (2017)) and multivariate systems (Bosman
37 et al. (2015)).

38 *1.1. Related Work*

39 Recent research has extended the scope of anomaly detection tasks to in-
40 clude root cause isolation governed by the development of explanatory meth-
41 ods capable of diagnosing and tracking faults across the system. Studies can
42 be split into two groups of distinct approaches. The first group approaches
43 explainability as the importance of individual features (Carletti et al. (2019)),
44 (Nguyen et al. (2019)), (Amarasinghe et al. (2018)). Those studies allow an
45 explanation of novelty by considering features independently. The second
46 group uses statistical learning creating models explainable via probability.
47 Yang et al. recently proposed a Bayesian network (BN) for fault detection
48 and diagnosis tasks. Individual nodes of the network represent normally
49 distributed variables, whereas the multiple regression model defines weights
50 and relationships. Using the predefined structure of the BN, the authors
51 propose an offline-trained model with online detection and diagnosis (Yang
52 et al. (2022)). Offline training, however, as we wrote earlier, do not allow
53 adaptation to expected novel pattern and, therefore, to our knowledge, is not
54 suitable for long-term operation on real IoT devices.

55 This paper emphasizes the importance of combining adaptability in in-
56 terpretable anomaly detection and proposes a method that addresses this
57 challenge. Here we report the discovery and characterization of an adaptive
58 anomaly detection method for streaming IoT data. The ability to diag-
59 nose multivariate data while providing root cause isolation, inherent in the
60 univariate case, extends our previous contribution to the field as presented
61 in (Wadinger and Kvasnica (2023)). The proposed algorithm represents a
62 general method for a broad range of safety-critical systems where anomaly
63 diagnosis and identification are paramount.

64 *1.2. Novelty of proposed approach*

65 The idea of using statistical outlier detection is well-established. We high-
66 lighting impactful contributions of (Yamanishi and Takeuchi (2002)) and (Ya-
67 manishi et al. (2004)). The authors propose a method for detecting anomalies
68 in a time series. The method is based on the assumption that the continuous
69 data is generated by a mixture of Gaussian distributions, while discrete data
70 is modeled as histogram density. The authors solve the problem of change
71 point detection as well. However, the adaptation system is unaware of such

72 changes, making the moving window the only source of adaptation. Our
73 self-supervised approach offers intelligent adaptation w.r.t. detected change
74 points. Moreover, the author of the study does not attempt to isolate the
75 root cause of the anomaly. We do so by computing the conditional proba-
76 bility of each measurement given the rest of the measurements and drawing
77 limits defining the normal event probability threshold.

78 A limited number of studies have focused on adaptation and interpretabil-
79 ity within the framework of anomaly detection. Two recent contributions
80 in this area are (Steenwinckel (2018)) and (Steenwinckel et al. (2021)). In
81 (Steenwinckel (2018)), the authors emphasize the importance of combining
82 prior knowledge with a data-driven approach to achieve interpretability, par-
83 ticularly concerning root cause isolation. They propose a novel approach
84 that involves extracting features based on knowledge graph pattern extrac-
85 tion and integrating them into the anomaly detection mechanism. This graph
86 is subsequently transformed into a matrix, and adaptive region-of-interest ex-
87 traction is performed using reinforcement learning techniques. To enhance
88 interpretability, a Generative Adversarial Network (GAN) reconstructs a new
89 graphical representation based on selected vectors. However, it's important
90 to note that the validation of this idealized approach is pending further in-
91 vestigation. Lately, (Steenwinckel et al. (2021)) introduced a comprehen-
92 sive framework for adaptive anomaly detection and root cause analysis in
93 data streams. While the adaptation process is driven by user feedback, the
94 specific mechanism remains undisclosed. The authors present an interpreta-
95 tion of their method through a user dashboard, featuring visualizations of
96 raw data. This dashboard is capable of distinguishing between track-related
97 problems and train-related issues, based on whether multiple trains at the
98 same geographical location approach the anomaly. Meanwhile, our attempts
99 aim to develop a self-supervised method capable of learning without human
100 supervision which is often limited in time and poses significant delays in
101 adaptation, while interpretation offers straightforward statistical reasoning
102 and root cause isolation.

103 *1.3. Validation*

104 Two case studies show that our proposed method, based on dynamic joint
105 normal distribution, has the capacity to explain novelties, isolate the root
106 cause of anomalies, and allow adaptation to change points, advancing recently
107 developed anomaly detection techniques for long-term deployment and cross-
108 domain usage. We observe similar detection performance, albeit with lower

109 scalability, when comparing our approach to well-established unsupervised
110 anomaly detection methods in streamed data which create a bedrock for
111 many state-of-the-art contributions, such as One-Class SVM (Amer et al.
112 (2013); Liu et al. (2014); Krawczyk and Woźniak (2015); Miao et al. (2019);
113 Gözüaçık and Can (2021)), and Half-Space Trees (Wetzig et al. (2019); Lyu
114 et al. (2020)).

115 *1.4. Broader Impact*

116 Potential applications of the proposed method are in the field of energy
117 storage systems, where the ability to detect anomalies and isolate their root
118 cause, whilst adapting to changes in operation and environment, is crucial
119 for the safety of the system. The proposed method is suitable for the existing
120 infrastructure of the system, allowing detection and diagnosis of the system
121 based on existing data streams. The dynamic process limits allow opera-
122 tional metrics monitoring, making potential early detection and prevention
123 easier. Using adaptable methods without interpretability, on the other hand,
124 may pose safety risks and lower total financial benefits, as the triggered false
125 alarms may need to be thoroughly analyzed, resulting in prolonged down-
126 times.

127 *1.5. Paper Organization*

128 The paper is structured as follows: We begin with the problem and mo-
129 tivation in **Section 1**, providing context. Next, in **Section 2**, we lay the
130 theoretical groundwork. Our proposed adaptive anomaly detection method is
131 detailed in **Section 3**. We then demonstrate real-world applications in **Sec-**
132 **tion 4**. Finally, we conclude the paper in **Section 5**, summarizing findings
133 and discussing future research directions.

134 The main contribution of the proposed solution to the developed body of
135 research is that it:

- 136 • Enriches interpretable anomaly detection with adaptive capabilities
- 137 • Identifies systematic outliers and root cause
- 138 • Uses self-learning approach on streamed data
- 139 • Utilizes existing IT infrastructure
- 140 • Establishes dynamic limits for signals

¹⁴¹ **2. Preliminaries**

¹⁴² In this section, we present the fundamental ideas that form the basis
¹⁴³ of the developed approach. Subsection 2.1 explains Welford's online algo-
¹⁴⁴ rithm, which can adjust distribution to changes in real-time. Subsection 2.2
¹⁴⁵ proposes a two-pass implementation that can reverse the impact of expired
¹⁴⁶ samples. The math behind distribution modeling in Subsection 2.3 estab-
¹⁴⁷ lishes the foundation for the Gaussian anomaly detection model discussed in
¹⁴⁸ Subsection 2.5, followed by conditional probability computation in Subsec-
¹⁴⁹ tion 2.4. The last subsection of the preliminaries is devoted to the definition
¹⁵⁰ of anomalies.

¹⁵¹ *2.1. Welford's Online Algorithm*

¹⁵² Welford introduced a numerically stable online algorithm for calculating
¹⁵³ mean and variance in a single pass. The algorithm allows the processing
¹⁵⁴ of IoT device measurements without the need to store their values Welford
¹⁵⁵ (1962).

¹⁵⁶ Given measurement x_i where $i = 1, \dots, n$ is a sample index in sample
¹⁵⁷ population n , the corrected sum of squares S_n is defined as

$$S_n = \sum_{i=1}^n (x_i - \bar{x}_n)^2, \quad (1)$$

¹⁵⁸ with the running mean \bar{x}_n defined as previous mean \bar{x}_{n-1} weighted by pro-
¹⁵⁹ portion of previously seen population $n - 1$ corrected by current sample as

$$\bar{x}_n = \frac{n-1}{n} \bar{x}_{n-1} + \frac{1}{n} x_n = \bar{x}_{n-1} + \frac{x_n - \bar{x}_{n-1}}{n}. \quad (2)$$

¹⁶⁰ Throughout this paper, we consider the following formulation of an update
¹⁶¹ to the corrected sum of squares:

$$S_n = S_{n-1} + (x_n - \bar{x}_{n-1})(x_n - \bar{x}_n), \quad (3)$$

¹⁶² as it is less prone to numerical instability due to catastrophic cancellation.
¹⁶³ Finally, the corresponding unbiased variance is

$$s_n^2 = \frac{S_n}{n-1}. \quad (4)$$

¹⁶⁴ This implementation of the Welford method requires the storage of three
¹⁶⁵ scalars: \bar{x}_{n-1} ; n ; S_n .

166 2.2. Inverse Welford's Algorithm

167 Based on (2), it is clear that the influence of the latest sample over the
 168 running mean decreases as the population n grows. For this reason, regulating
 169 the number of samples used for sample mean and variance computation
 170 has crucial importance over adaptation. Given access to the instances used
 171 for computation and expiration period $t_e \in \mathbb{N}_0^{n-1}$, reverting the impact of
 172 x_{n-t_e} can be written as follows

$$S_{n-1} = S_n - (x_{n-t_e} - \bar{x}_{n-1})(x_{n-t_e} - \bar{x}_n), \quad (5)$$

173 where the reverted mean is given as

$$\bar{x}_{n-1} = \frac{n}{n-1}\bar{x}_n - \frac{1}{n-1}x_{n-t_e} = \bar{x}_n - \frac{x_{n-t_e} - \bar{x}_n}{n-1}. \quad (6)$$

174 Finally, the unbiased variance follows the formula:

$$s_{n-1}^2 = \frac{S_{n-1}}{n-2}. \quad (7)$$

175 2.3. Statistical Model of Multivariate System

176 Multivariate normal distribution generalizes the multivariate systems to
 177 the model where the degree to which variables are related is represented by
 178 the covariance matrix. Gaussian normal distribution of variables is a reasonable
 179 assumption for process measurements, as it is a common distribution
 180 that arises from stable physical processes measured with noise. The general
 181 notation of multivariate normal distribution is:

$$\mathbf{X} \sim \mathcal{N}_k(\boldsymbol{\mu}, \boldsymbol{\Sigma}), \quad (8)$$

182 where k -dimensional mean vector is denoted as $\boldsymbol{\mu} = (\bar{x}_1, \dots, \bar{x}_k)^T \in \mathbb{R}^k$
 183 and $\boldsymbol{\Sigma} \in \mathbb{R}^{k \times k}$ is the $k \times k$ covariance matrix, where k is the index of last
 184 random variable.

185 The probability density function (PDF) $f(\mathbf{x}; \boldsymbol{\mu}, \boldsymbol{\Sigma})$ of multivariate normal
 186 distribution is denoted as:

$$f(\mathbf{x}; \boldsymbol{\mu}, \boldsymbol{\Sigma}) = \frac{1}{(2\pi)^{k/2}|\boldsymbol{\Sigma}|^{1/2}} e^{-\frac{1}{2}(\mathbf{x}-\boldsymbol{\mu})^\top \boldsymbol{\Sigma}^{-1}(\mathbf{x}-\boldsymbol{\mu})}, \quad (9)$$

187 where \mathbf{x} is a k -dimensional vector of measurements x_i at time i , $|\boldsymbol{\Sigma}|$
 188 denotes the determinant of $\boldsymbol{\Sigma}$, and $\boldsymbol{\Sigma}^{-1}$ is the inverse of $\boldsymbol{\Sigma}$.

189 The cumulative distribution function (CDF) of a multivariate Gaussian
 190 distribution describes the probability that all components of the random ma-
 191 trix \mathbf{X} take on a value less than or equal to a particular point \mathbf{x} in space,
 192 and can be used to evaluate the likelihood of observing a particular set of
 193 measurements or data points. The CDF is often used in statistical applica-
 194 tions to calculate confidence intervals, perform hypothesis tests, and make
 195 predictions based on observed data. In other words, it gives the probability
 196 of observing a random vector that falls within a certain region of space. The
 197 standard notation of CDF is as follows:

$$F(\mathbf{x}; \boldsymbol{\mu}, \boldsymbol{\Sigma}) = \int_{-\infty}^{\mathbf{x}} f(\mathbf{x}; \boldsymbol{\mu}, \boldsymbol{\Sigma}) d\mathbf{x}, \quad (10)$$

198 where $d\mathbf{x}$ denotes the integration over all k dimensions of \mathbf{x} .

199 As the equation (10) cannot be integrated explicitly, an algorithm for
 200 numerical computation was proposed in Genz (2000).

201 Given the PDF, we can also determine the value of \mathbf{x} that corresponds to a
 202 given quantile q using a numerical method for inversion of CDF (ICDF) often
 203 denoted as percent point function (PPF) or $F(\mathbf{x}; \boldsymbol{\mu}, \boldsymbol{\Sigma})^{-1}$. An algorithm that
 204 calculates the value of the PPF for univariate normal distribution is reported
 205 below as Algorithm 1.

Algorithm 1 Percent-Point Function for Normal Distribution

Input: quantile q , sample mean \bar{x}_n (2), sample variance s_n^2 (4)

Output: threshold value $\tilde{x}_{q,n}$

Initialisation :

1: $f \leftarrow 10; l \leftarrow -f; r \leftarrow f;$

LOOP Process

2: **while** $F(l; \bar{x}_n, s_n^2) > 0$ **do**

3: $r \leftarrow l;$

4: $l \leftarrow lf;$

5: **end while**

6: **while** $F_X(r) - q < 0$ **do**

7: $l \leftarrow r;$

8: $r \leftarrow rf;$

9: **end while**

10: $\tilde{x}_{q,n} = \arg \min_{x_n} \|F(x_n; \bar{x}_n, s_n^2) - q\|$ s.t. $l \leq x_n \leq r$

11: **return** $\tilde{x}_{q,n} \sqrt{s_n^2 + \bar{x}_n}$

206 The Algorithm 1 for PPF computation is solved using an iterative root-
 207 finding algorithm such as Brent's method Brent (1972).

208 *2.4. Conditional Probability Distribution*

209 Considering that we observe particular vector \mathbf{x}_i , we can update probabil-
 210 ity distributions, calculated according to the rules of conditional probability,
 211 of individual measurements within the vector given the rest of the measure-
 212 ments in \mathbf{x}_i . Let's assume multivariate normal distribution (8) and without
 213 loss of generality, that the vector \mathbf{x}_i can be partitioned into subset variable
 214 x_a , and complement vector \mathbf{x}_b as follows

$$\mathbf{x}_i = \begin{bmatrix} x_a \\ \mathbf{x}_b \end{bmatrix} \text{ with dimensions } \begin{bmatrix} 1 \times 1 \\ (k-1) \times 1 \end{bmatrix}, \quad (11)$$

215 where $a = 1, \dots, k$ and $\mathbf{b} = \{1, 2, \dots, k\}$ where $a \notin \mathbf{b}$. This partitioning
 216 allows us to define block-wise mean and covariance as follows:

$$\boldsymbol{\mu} = \begin{bmatrix} \mu_a \\ \boldsymbol{\mu}_b \end{bmatrix} \text{ with dimensions } \begin{bmatrix} 1 \times 1 \\ (k-1) \times 1 \end{bmatrix}, \quad (12)$$

217 and

$$\boldsymbol{\Sigma} = \begin{bmatrix} \sigma_{aa}^2 & \boldsymbol{\Sigma}_{ab} \\ \boldsymbol{\Sigma}_{ba} & \boldsymbol{\Sigma}_{bb} \end{bmatrix} \text{ with dimensions } \begin{bmatrix} 1 \times 1 & 1 \times (k-1) \\ (k-1) \times 1 & (k-1) \times (k-1) \end{bmatrix}. \quad (13)$$

218 where a and \mathbf{b} represent distinct components within the vector.

219 Subsequently, we can derive the conditional distribution of any subset
 220 variable x_a , given the complementary vector \mathbf{x}_b . This conditional distribution
 221 conforms to a univariate normal distribution, characterized by:

$$X_a | \mathbf{X}_b \sim \mathcal{N}(\mu_{a|\mathbf{b}}, \sigma_{a|\mathbf{b}}^2). \quad (14)$$

222 where $\mu_{a|\mathbf{b}}$ denotes the conditional mean and $\sigma_{a|\mathbf{b}}^2$ represents the condi-
 223 tional variance. These crucial parameters can be computed using the Schur
 224 complement.

225 For a general matrix M expressed as:

$$M = \begin{bmatrix} A & B \\ C & D \end{bmatrix}, \quad (15)$$

226 the Schur complement of the block matrix M is denoted as:

$$M \mid D = A - BD^{-1}C. \quad (16)$$

227 Applying Equation (16), we can calculate the conditional variance $\sigma_{a|b}^2$
 228 using the covariance matrix notation from Equation (13) as follows:

$$\sigma_{a|b}^2 = \sigma_{aa}^2 - \Sigma_{ab}\Sigma_{bb}^{-1}\Sigma_{ba}, \quad (17)$$

229 while the conditional mean, denoted as $\mu_{a|b}$, is determined by:

$$\mu_{a|b} = \mu_a + \Sigma_{ab}\Sigma_{bb}^{-1}(\mathbf{x}_b - \boldsymbol{\mu}_b). \quad (18)$$

230 It is important to note that Σ_{bb}^{-1} in Equations (17) and (18) signifies
 231 the inverse of the covariance matrix Σ_{bb} . Thus, the conditional variance
 232 $\sigma_{a|b}^2$ essentially represents the Schur complement of Σ_{bb} within the overall
 233 covariance matrix Σ .

234 2.5. Gaussian Anomaly Detection

235 From a viewpoint of statistics, outliers are commonly denoted as values
 236 that significantly deviate from the mean. Under the assumption that the
 237 spatial and temporal characteristics of a system, observed over a moving
 238 window, can be suitably represented as normally distributed features, we
 239 assert that any anomaly can be identified as an outlier.

240 From a statistical viewpoint, outliers can be denoted as values that sig-
 241 nificantly deviate from the mean. Assuming that the spatial and temporal
 242 characteristics of the system over the moving window can be encoded as nor-
 243 mally distributed features, we can claim, that any anomaly may be detected
 244 as an outlier.

245 In empirical fields like machine learning, the three-sigma rule (3σ) pro-
 246 vides a framework for characterizing the region of a distribution within which
 247 normal values are expected to fall with high confidence. This rule renders
 248 approximately 0.265% of values in the distribution as anomalous.

249 The 3σ rule establishes the probability that any sample x_a of a random
 250 vector X lies within a given CDF over a semi-closed interval as the distance
 251 from the conditional mean $\mu_{a|b}$ of 3 conditional variances $\sigma_{a|b}^2$ and gives an
 252 approximate value of q as

$$q = P\{|x_a - \mu_{a|b}| < 3\sigma_{a|b}^2\} = 0.99735. \quad (19)$$

253 Utilizing a probabilistic model of normal behavior, we can determine
 254 threshold values x_l and x_u corresponding to the closed interval of the CDF

255 where this probability is established. The inversion of Equation (10) facilitates
 256 this calculation, yielding:

$$x_l = F((1 - P\{|x_a - \mu_{a|\mathbf{b}}| < 3\sigma_{a|\mathbf{b}}^2\}); \mu_{a|\mathbf{b}}, \sigma_{a|\mathbf{b}}^2)^{-1}, \quad (20)$$

257 for the lower limit, and

$$x_u = F((P\{|x_a - \mu_{a|\mathbf{b}}| < 3\sigma_{a|\mathbf{b}}^2\}); \mu_{a|\mathbf{b}}, \sigma_{a|\mathbf{b}}^2)^{-1}, \quad (21)$$

258 for the upper limit. These lower and upper limits together form vectors
 259 \mathbf{x}_l and \mathbf{x}_u , respectively, defining the region of normal system operation. This
 260 region is conceptualized as a hypercube in the feature space, with each di-
 261 mension bounded by the corresponding feature limits, as computed using
 262 Equations (20) and (21) for all $a = 1, \dots, k$; $\mathbf{b} = \{1, 2, \dots, k\}$ where $a \notin \mathbf{b}$.

263 Such threshold is computed for each feature of the system, resulting in
 264 a vector of lower and upper limits. The vector of limits is used to define
 265 the region of normal operation of the system. The region is defined as a
 266 hypercube in the feature space, where each dimension is defined by the limits
 267 of the corresponding feature.

268 The predicted state of the system, denoted as y_i , and the presence of
 269 anomalies in signals $\mathbf{y}_{s,i}$ at time i are determined based on the maximum
 270 distance of observations from the center of the hypercube. The center of the
 271 hypercube corresponds to the vector of conditional means $\mu_{a|\mathbf{b}}$ with respect
 272 to other features. The calculation of this distance involves the cumulative
 273 distribution function (CDF) of observations and conditional distributions, as
 274 follows:

$$F(x_a; \mu_{a|\mathbf{b}}, \sigma_{a|\mathbf{b}}^2) : a = 1, \dots, k; \mathbf{b} = \{1, 2, \dots, k\} \text{ where } a \notin \mathbf{b}. \quad (22)$$

275 Subsequently, anomalies in individual inputs are defined as follows:

$$\mathbf{y}_{s,i} = \begin{cases} 0 & \text{if } T \leq (22) \\ 1 & \text{if } T > (22), \end{cases} \quad (23)$$

276 where T represents a threshold that distinguishes between normal signal
 277 measurement ($\mathbf{y}_{s,i} = 0$) and abnormal ($\mathbf{y}_{s,i} = 1$).

278 For the predicted state of the system, the maximum value from $\mathbf{y}_{s,i}$ is
 279 considered, resulting in:

$$y_i = \begin{cases} 1 & \text{if } 1 \in \mathbf{y}_{s,i} \\ 0 & \text{otherwise,} \end{cases} \quad (24)$$

defining the discrimination boundary between system operation where $y_i = 0$ indicates normal system operation, and $y_i = 1$ indicates anomalous operation.

2.6. Anomaly Definition

In the realm of data analysis, anomalies are conspicuous deviations from the anticipated patterns within a dataset. Traditionally, the task of anomaly detection has relied upon unsupervised methodologies, wherein the identification of "outliers" entails the comparison of data points in both temporal and spatial contexts. This approach, often referred to as point-wise anomaly detection, classifies a data point as an anomaly when it exhibits significant dissimilarity from its neighboring data points (Iglesias Vázquez et al. (2023)).

The concept of point anomalies, influenced by factors such as temporal and spatial aspects, can be further categorized into conditional and contextual anomalies (Ruff et al. (2021)).

Nevertheless, this conventional method may not be suitable for scenarios characterized by collective anomalies, where clusters of abnormal data points coexist. A more pragmatic approach defines anomalies as deviations from established "normal" patterns, resembling the principles of semi-supervised learning. Change point detection, in a similar vein, can be regarded as a relative approach that takes into account the varying dynamics of changes, whether they occur gradually or abruptly (Iglesias Vázquez et al. (2023)).

It is imperative to recognize that the interpretation of anomalies, outliers, and novelties can vary upon the application. Anomalies typically garner significant attention, while outliers are often treated as undesirable noise and are typically excluded during data preprocessing. Novelties, on the other hand, signify new observations that necessitate model updates to adapt to an evolving environment (Ruff et al. (2021)).

Notwithstanding the differences in terminology, methods employed for the identification of data points residing in low-probability regions, irrespective of whether they are referred to as "anomaly detection," "outlier detection," or "novelty detection," share fundamental similarities (Iglesias Vázquez et al. (2023)).

312 **3. Novelty Detection and Interpretation Framework**

313 In this section, we propose an adaptive and interpretable detection frame-
314 work for multivariate systems with streaming IoT devices. This approach
315 models the system as a dynamic joint normal distribution, enabling it to ef-
316 fectively adapt to pervasive nonstationary effects on processes. Our method
317 handles various factors, including change points, concept drift, and seasonal
318 effects. Our primary contribution lies in the fusion of an adaptable self-
319 supervised system with root cause identification capabilities. This combi-
320 nation empowers the online statistical model to diagnose anomalies through
321 two distinct avenues. Firstly, it employs conditional probability calculations
322 to assess the system’s operating conditions’ normality. Secondly, it identifies
323 outliers within individual signal measurements and features based on dy-
324 namic alert-triggering process limits. In the following sections, we describe
325 our proposed methodology across three subsections. The initial subsection
326 delves into the process of initializing the model’s parameters. The subsequent
327 section describes online training and adaptation, while the final subsection
328 expounds upon the model’s detection and diagnostic capabilities. For a con-
329 cise representation of the proposed method, Algorithm 2 is provided.

330 *3.1. Model Parameters Initialization*

331 The model initialization is governed by defining two tunable hyperparam-
332 eters of the model: the expiration period (t_e) and the threshold (T). The
333 expiration period determines the window size for time-rolling computations,
334 impacting the proportion of outliers within a given timeframe, and directly
335 influencing the relaxation (with a longer expiration period) or tightening
336 (with a shorter expiration period) of dynamic signal limits. Additionally, we
337 introduce a grace period, which defaults to $3/4t_e$, allowing for model calibra-
338 tion. During this grace period, system anomalies are not flagged to prevent
339 false positives and speed up self-supervised learning in Subsection 3.2. The
340 length of the expiration period inversely correlates with the model’s ability
341 to adapt to sudden changes. The adaptation to shifts in the data-generating
342 process, such as changes in mean or variance, is managed through the adapta-
343 tion period t_a . A longer t_a results in slower adaptation but potentially longer
344 alerts, which can be valuable during extended outlier periods. In most cases,
345 $t_a = 1/4t_e$ offers optimal performance.

346 As a general rule of thumb, expiration period t_e should be determined
347 based on the slowest observed dynamics within the multivariate system. The

348 threshold T defaults to the three-sigma probability of q in (19). Adjusting
 349 this threshold can fine-tune the trade-off between precision and recall. A
 350 higher threshold boosts recall but may lower precision, while a lower thresh-
 351 old enhances precision at the cost of recall. The presence of one non-default
 352 easily interpretable hyperparameter facilitates adaptability to various sce-
 353 narios. We recommend starting with the default values of other parameters
 354 and making adjustments based on real-time model performance.

355 *3.2. Online training*

356 Training in RAID follows an incremental learning approach, processing
 357 each new sample upon arrival. Incremental learning allows online parame-
 358 ter updates, albeit with a potential computational delay affecting response
 359 latency.

360 In the case of a dynamic joint probability distribution, the parameters are
 361 μ_i and Σ_i at time instance i . Update of the mean vector μ_i and covariance
 362 matrix Σ_i is governed by Welford's online algorithm using equation (2) and
 363 (4) respectively. Samples beyond the expiration period t_e are disregarded
 364 during the second pass. The effect of expired samples is reverted using inverse
 365 Welford's algorithm for mean (6) and variance (7), accessing the data in the
 366 buffer. For details, refer to Subsection 2.2.

367 It's worth noting that adaptation relies on two self-supervised methods.
 368 Adaptation routine runs if the observation at time instance i is considered
 369 normal. Adaptation period t_a allows the model to update the distribution
 370 on outliers as well. Given the predicted system anomaly state from (24) as
 371 y_i over the window of past observations $\mathbf{y}_i = \{y_{i-t_a}, \dots, y_i\}$, the following test
 372 holds when adaptation is performed on outlier:

$$\frac{\sum_{y \in \mathbf{y}_i} y}{n(\mathbf{y}_i)} > 2 * (T - 0.5). \quad (25)$$

373 Here $n(\mathbf{y}_i)$ denotes the dimensionality of \mathbf{y}_i . The logic of the (25) follows the
 374 probabilistic approach to anomalies that assumes a number of anomalies are
 375 lower or equal to the conditional probability at both tails of the distribution

376 *3.3. Online prediction*

377 In the prediction phase, multiple metrics are evaluated to assess the state
 378 of the modeled system.

379 Firstly, we calculate the parameters of the conditional distribution con-
 380 cerning the dynamic multivariate Gaussian distribution. These calculations

381 are performed for the process observation vector \mathbf{x}_i at time instance i . Specifically,
382 we compute the conditional mean using (18) and the conditional variance
383 using (17). These computations yield univariate conditional distributions
384 for individual signals and features. These conditional distributions play
385 a crucial role in assessing the abnormality of signals and features concerning
386 other observed values. This assessment relies on the strength of relationships
387 defined by the covariance matrix of the dynamic multivariate Gaussian
388 distribution. Consequently, our approach inherently considers the interactions
389 between input signals and features. The determination of anomalous
390 behavior is governed by (23).

391 Any anomaly detected within one of the features triggers an alert at the
392 system level. The decision regarding the overall system's anomalous behavior
393 is guided by (24). Nevertheless, individual determinations of anomalies serve
394 as a diagnostic tool for isolating the root cause of anomalies.

395 To assist operators in their assessments, we establish a hypercube defined
396 by lower and upper threshold values, denoted as \mathbf{x}_l and \mathbf{x}_u , respectively.
397 These thresholds are derived from (20) and (21), incorporating updated
398 model parameters. Lower and upper thresholds play a pivotal role as dynamic
399 process limits. They replace the conservative process limits provided
400 in sensor documentation, accounting for factors such as aging and actual
401 environmental conditions that influence sensor operation.

402 Our framework anticipates unexpected novel behavior, including signal
403 loss. This anticipation involves calculating the cumulative distribution function
404 (CDF) over the univariate normal distribution of sampling, focusing
405 on the differences between subsequent timestamps. We operate under the
406 assumption that, over the long term, the distribution of sampling times remains
407 stable. As a result, we employ a one-pass update mechanism utilizing (2) and (4). To proactively detect subtle changes in sampling patterns,
408 self-supervised learning is employed, leveraging anomalies weighted by the
409 deviation from $(1 - F(x_i; \mu, \sigma^2))$ for training.

411 The system is vigilant in identifying change points. When the adaptation
412 test specified in (25) is satisfied, change points are flagged and isolated. This
413 initiation of change points triggers updates to the model, ensuring it adapts
414 to evolving data patterns effectively.

Algorithm 2 Online Detection and Identification Workflow

Input: expiration period t_e

Output: system anomaly y_i , signal anomalies $\mathbf{y}_{s,i}$, sampling anomaly $y_{t,i}$, change-point $y_{c,i}$, lower thresholds $\mathbf{x}_{l,i}$, upper thresholds $\mathbf{x}_{u,i}$,

Initialisation :

- 1: $i \leftarrow 1; n \leftarrow 1; T \leftarrow (19); \boldsymbol{\mu} \leftarrow \mathbf{x}_0; \boldsymbol{\Sigma} \leftarrow \mathbf{1}_{k \times k}; \mu_t \leftarrow 0; \sigma_t^2 \leftarrow 1;$
 - 2: compute $F(\mathbf{x}_0; \boldsymbol{\mu}, \boldsymbol{\Sigma})$ using algorithm in Genz (2000);
LOOP Process
 - 3: **loop**
 - 4: $\mathbf{x}_i, t_i \leftarrow \text{RECEIVE}();$
 - 5: $\mathbf{y}_{s,i} \leftarrow \text{PREDICT}(\mathbf{x}_i, T)$ using (23);
 - 6: $y_i \leftarrow \text{PREDICT}(\mathbf{y}_{s,i})$ using (24);
 - 7: $\mathbf{x}_{l,i}, \mathbf{x}_{u,i} \leftarrow \text{GET}(T, \boldsymbol{\mu}, \boldsymbol{\Sigma})$ using Algorithm 1;
 - 8: $y_{t,i} \leftarrow \text{PREDICT}(t_i - t_{i-1})$ using (23);
 - 9: $\mu_t, \sigma_t^2 \leftarrow \text{UPDATE}(t_i - t_{i-1}, \mu_t, \sigma_t^2)$ using (2), (4);
 - 10: **if** not (24) **or** (25) **then**
 - 11: $\boldsymbol{\mu}, \boldsymbol{\Sigma} \leftarrow \text{UPDATE}(\mathbf{x}_i, \boldsymbol{\mu}, \boldsymbol{\Sigma}, n)$ using (2), (4);
 - 12: **if** (25) **then**
 - 13: $y_{c,i} \leftarrow 1;$
 - 14: **else**
 - 15: $y_{c,i} \leftarrow 0;$
 - 16: **end if**
 - 17: $n \leftarrow n + 1;$
 - 18: **for** \mathbf{x}_{i-t_e} **do**
 - 19: $\boldsymbol{\mu}, \boldsymbol{\Sigma} \leftarrow \text{REVERT}(\mathbf{x}_{i-t_e}, \boldsymbol{\mu}, \boldsymbol{\Sigma}, n)$ using (6), (7);
 - 20: $n \leftarrow n - 1;$
 - 21: **end for**
 - 22: **end if**
 - 23: $i \leftarrow i + 1;$
 - 24: **end loop**
-

⁴¹⁵ **4. Case Study**

⁴¹⁶ This section provides a benchmark and two case studies that showcase
⁴¹⁷ the effectiveness and applicability of our proposed approach. In the following
⁴¹⁸ Subsections, we investigate the properties and performance of the approach
⁴¹⁹ using streamed benchmark system data and signals from IoT devices in a mi-

420 crogrid system. The successful deployment demonstrates that this approach
421 is suitable for existing process automation infrastructure.

422 The case studies were realized using Python 3.10.1 on a machine employ-
423 ing an 8-core Apple M1 CPU and 8 GB RAM.

424 *4.1. Benchmark*

425 In this subsection, we compare the proposed method with adaptive un-
426 supervised detection methods without an interpretability layer. Two of the
427 well-established methods, providing iterative learning capabilities over mul-
428 tivariate time-series data are One-Class Support Vector Machine (OC-SVM)
429 and Half Spaced Trees (HS-Trees). Both methods represent the backbone
430 of multiple state-of-the-art methods for cases of anomaly detection on dy-
431 namic system data, with a brief list of recent applications in Introduction
432 1.3. Comparison is conducted on real benchmarking data, annotated with
433 labels of whether the observation was anomalous or normal. The dataset of
434 Skoltech Anomaly Benchmark (SKAB) Katser and Kozitsin (2020) is used for
435 this purpose, as no established benchmarking multivariate data were found
436 regarding energy storage systems. It represents a combination of experiments
437 with the behavior of rotor imbalance as a subject to various functions intro-
438 duced to control action as well as slow and sudden changes in the amount
439 of water in the circuit. The system is described by 8 features. The data
440 were preprocessed according to best practices for the given method, namely:
441 standard scaling for OC-SVM, normalization for HS-Trees, and no scaling
442 for our proposed method. The optimal quantile threshold value for both
443 reference methods is found using Bayesian Optimization. Due to no further
444 knowledge about the process, the parameters of the proposed method were
445 optimized using Bayesian Optimization as well. Results are provided within
446 Table 1, evaluating F1 score, Recall and Precision. A value of 100% at each
447 metric represents a perfect detection. The latency represents the average
448 computation time per sample of the pipeline including training and data
449 preprocessing.

450 The results in Table 1 suggest, that our algorithm provides slightly better
451 performance than reference methods. Based on the Scoreboard for various
452 algorithms on SKAB’s Kaggle page, our iterative approach performs com-
453 parably to the evaluated batch-trained model. Such a model has all the
454 training data available before prediction unlike ours, evaluating the metrics
455 iteratively on a streamed dataset.

Table 1: Metrics evaluation on SKAB dataset

Metric	AID	OC-SVM	HS-Trees
F1 [%]	48.70	44.42	34.10
Recall [%]	49.90	56.67	32.57
Precision [%]	47.56	36.52	35.77
Avg. Latency [ms]	1.55	0.44	0.21

456 *4.2. Battery Energy Storage System (BESS)*

457 In the first case study, we verify our proposed method on BESS. The
 458 BESS reports measurements of State of Charge (SoC), supply/draw energy
 459 set-points, and inner temperature, at the top, middle, and bottom of the
 460 battery module. Tight battery cell temperature control is needed to optimize
 461 performance and maximize the battery’s lifespan. Identifying anomalous
 462 events and removal of corrupted data might yield significant improvement
 463 in the process control level and increase the reliability and stability of the
 464 system.

465 The default sampling rate of the signal measurement is 1 minute. How-
 466 ever, network communication of the IoT devices is prone to packet dropout,
 467 which results in unexpected non-uniformities in sampling. The data are
 468 normalized to the range $[0, 1]$ to protect the sensitive business value. The
 469 proposed approach is deployed to the existing infrastructure of the system,
 470 allowing real-time detection and diagnosis of the system.

471 The industrial partner provided a physical model of the battery cell tem-
 472 perature, defined as follows:

$$\begin{aligned} T_{\text{bat},i+1} = & T_{\text{bat},i} + T_s(q_{\text{fan}}V_{\text{b,max}}\rho c_p(T_{\text{out}} - T_{\text{bat},i}) + V_{\text{c,max}}q_{\text{circ,fan}}\rho c_p T_{\text{bat},i} \\ & + q_{\text{circ,fan}}(P_{\text{cool}}q_{\text{cool}}P_{\text{heat}}q_{\text{heat}}) + c_{\text{scale}}Q_{\text{bat}} + q_{\text{inner fans}} \\ & - (V_{\text{b,max}}q_{\text{fan}}V_{\text{c,max}}q_{\text{circ,fan}})\rho c_p T_{\text{bat},i})/(m_{\text{bat}}c_{\text{p,b}}) \end{aligned} \quad (26)$$

473 When combined with an averaged measurement of battery cell temper-
 474 ature, we could compute the difference between real and predicted temper-
 475 ature. Such deviation can be useful in detecting unexpected patterns in
 476 temperature. Nevertheless, it may be inaccurate as the physical model is
 477 simplified and does not account for spatial aspects, like temperature gra-
 478 dients as well as different dynamic effects of charging and discharging on

479 temperature. Therefore, the raw measured temperature is used as well. The
480 deviation between demanded power and delivered power was used to aid the
481 identification of the state, as the increased difference might be related to
482 other unexpected and novel patterns.

483 Fig. 1 depicts the operation of the BESS over March 2022. Multiple
484 events of anomalous behavior happened within this period, confirmed by the
485 operators, that are observable through a sudden or significant shift in mea-
486 surements in a given period. As the first step, the detection mechanism was
487 initialized, following the provided guidelines for parameter selection in Sub-
488 section 3.1. The expiration period was set to $t_e = 7$ days, due to the weekly
489 seasonality of human behavior impacting battery usage. The threshold was
490 kept at default value $T = 0.99735$. A grace period, during which the model
491 learns from both normal and anomalous data (though normal are expected),
492 is shortened to 2.5 days to observe the effect of BESS calibration happening
493 on 3rd day from deployment.

494 The deployment and operation of the anomaly detection system were suc-
495 cessful as shown by its adaptation of changepoint on 7th March 2022 that
496 appeared due to the relocation of the battery storage system outdoors. The
497 model was adapted online based on Subsection 3.2. The sudden shift in envi-
498 ronmental conditions, due to the transfer of the system to outside changed the
499 dynamics of the system's temperature. However, new behavior was adopted
500 by the top-level anomaly isolation system within five days, reducing potential
501 false alerts afterward, by observably shifting the conditional mean to lower
502 temperatures. Perhaps more interesting are the alerted changepoints.

503 Calibration of the BESS, usually observed as deviations of setpoint from
504 real power demand and multiple peaks in temperature was captured as well.

505 The system identified 6 deviations in sampling, denoted by the red bars
506 in Fig. 1. 4 anomalies with shorter duration represented packet loss. The
507 prolonged anomaly was notified during the transfer of the battery pack. The
508 longest dropout observed happened across 20th March up to 21st. Unexpect-
509 edly, the change point detection module triggered an alarm at the end of
510 the loss, resulting in adaptation and a sharp shift in drawn limits for Power
511 Setpoint Deviation. Red dots represent anomalies at the signal level given
512 by equation (23). The dynamic signal limits are surpassed in one or multiple
513 signals during the system's anomalies. The root cause isolation allows the
514 pairing of anomalies with specific features. Conditional probability, against
515 which the anomalies are evaluated allows consideration of signal relationships
516 within individual limits.

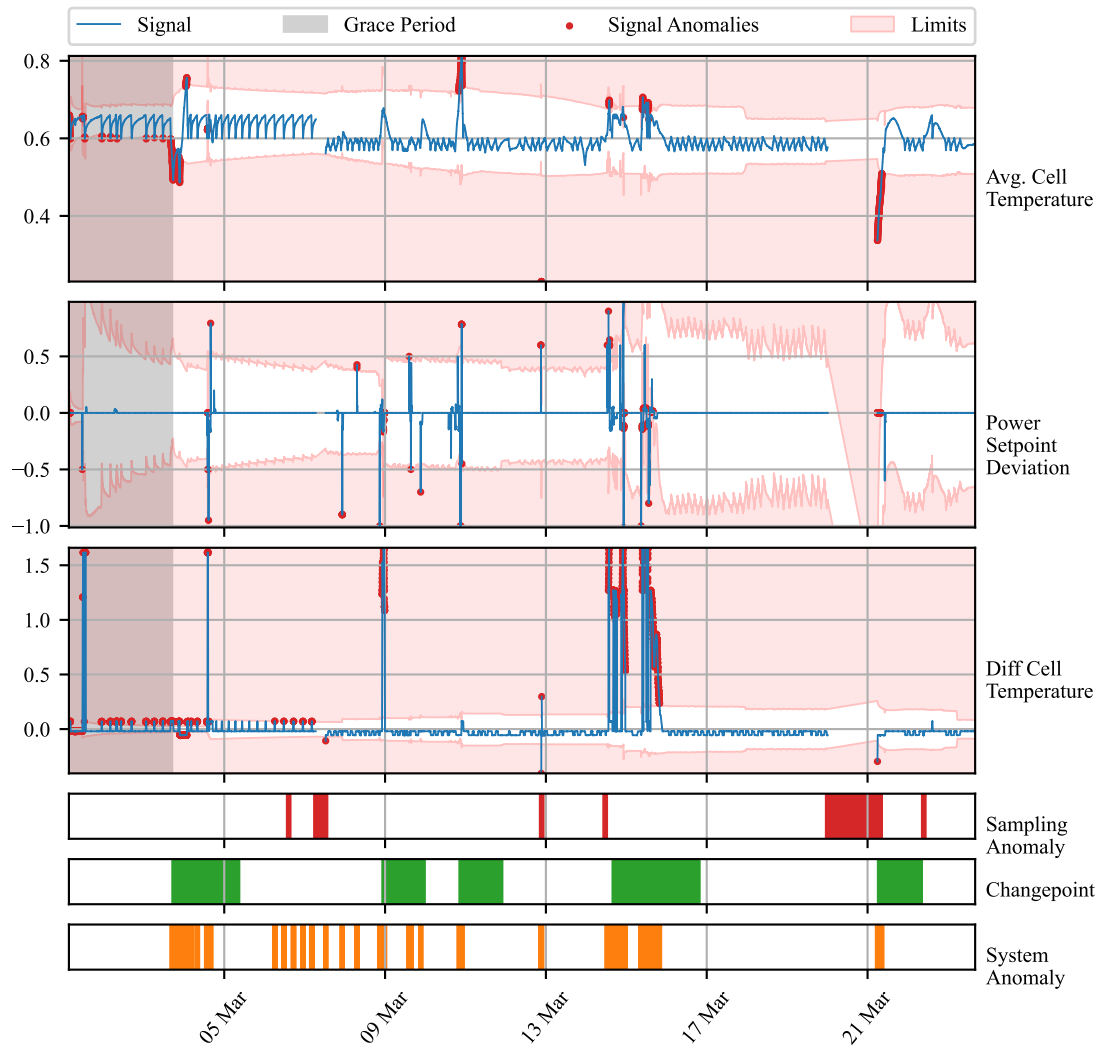


Figure 1: Time Series of BESS measurements (blue line) of process variables. The y-axis renders the values after the normalization of raw inputs. Root causes of anomalies are marked within specific signals as red dots. The light red area represents out-of-limits values for individual signals. Non-uniform sampling is marked as red bars. Green bars represent the times, at which changepoint was detected. All the signal anomalies are depicted as orange bars below the graph.

517 *4.3. Kokam Battery Temperature Module(BESS)*

518 A second case study is concerned with monitoring temperature profiles of
519 individual modules of battery pack deployed at end user. During the oper-
520 ation, a hardware fault of the cooling fan happened. Our industrial partner
521 was interested in finding out, whether such an event could be captured by
522 an anomaly detection system. The data for 12 modules, each coming with 6
523 channels of measurement were retrieved in 30-second sampling and processed
524 in a streamed manner. We found it informative to compute the deviation
525 of the observed value from the average of all the above-mentioned measure-
526 ments.

527 Our anomaly detection system was, once again, initialized with an ex-
528 piration period of 7 days. The grace period was shortened to 1 day. The
529 threshold value was shifted to a 4 sigma value of 99.977% to minimize the
530 number of alarms.

531 In Figure 2 we observe 5 days of deviations between the observed tem-
532 perature measured by channels of module 9 and the average temperature
533 of all modules. After the grace period, we observe multiple system alarms
534 raised by various channels. Until the noon of 22nd August, they seem to be
535 spread out randomly between individual channels. During the late evening
536 of 22nd, anomalies were reported by both channels 4 and 5 for a prolonged
537 period, followed by an anomalous rise in temperature measured by channel
538 6 early in the morning on 23rd August. The fan fault was observed approx-
539 imately at 5 pm on 23rd August. Our anomaly detection system instantly
540 raised an alarm, notifying us of anomalous behavior reported by channels 1
541 - 3. The prolonged duration of the alarm triggered the changepoint alarm
542 approximately 2 hours later. This resulted in a slightly faster adaptation of
543 the system to the new operation under increased temperature. Surprisingly,
544 the temperature decreased during the next day, notifying us of the fan being
545 in operation, to fail again 30 minutes later after the battery modules were
546 cooled down to the previous setpoint. The anomaly detection system was
547 triggered once again, although adaptation loosened the region of normal op-
548 eration to allow itself to adapt. No significant anomalies in sampling were
549 observed during the period.

550 **5. Conclusion**

551 In this paper, we examine the capacity of adaptive conditional probability
552 distribution to model the normal operation of dynamic systems employing

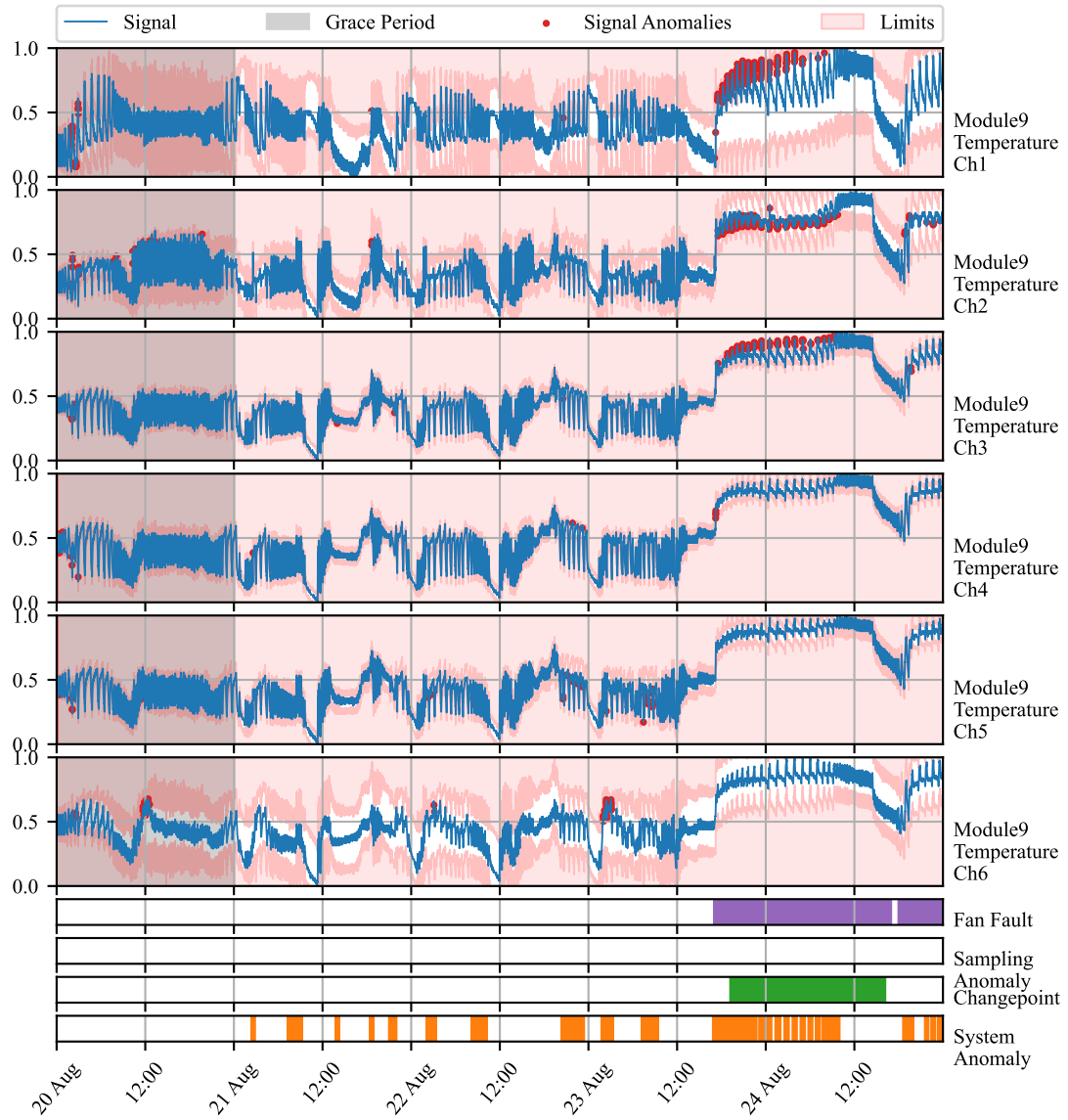


Figure 2: Time Series of BESS measurements (green line) of process variables. Non-uniform ticks on the x-axis mark days of interest (NOTE: some marks are hidden due to the readability). The y-axis renders the normalized process variables. System anomalies are marked as red dots. Non-uniform sampling is detected at blue vertical lines. Yellow vertical lines denote changepoint adaptation

553 streaming IoT devices and isolate the root cause. The dynamics of the sys-
554 tems are elaborated in the model using Welford’s online algorithm with the
555 capacity to update and revert sufficient parameters of underlying multivariate
556 Gaussian distribution in time making it possible to elaborate non-stationarity
557 in the process variables. Moreover, the self-supervision allows protection of
558 the distribution from the effect of outliers and increased speed of adaptation
559 in cases of changes in operation.

560 We assume the Gaussian distribution of measurements over a bounded
561 time frame related to the system dynamics. We consider such an assumption
562 reasonable, with support of multiple trials where the Kolmogorov-Smirnov
563 test did not reject this hypothesis. The statistical model provides the capac-
564 ity for the interpretation of the anomalies as extremely deviating observations
565 from the mean vector. Another assumption held in this study is that any
566 anomaly, spatial or temporal, can be transformed in such a way that makes
567 it an outlier given that we expose such effects as features as shown in case
568 studies.

569 Our approach establishes the system’s operation state at the global anomaly
570 level by considering interactions between input measurements and engineered
571 features and computing distance from conditional probability. At the second
572 level, dynamic process limits based on PPF at threshold probability, given
573 multivariate distribution parameters, help isolate the root cause of anom-
574 alies. This level serves the diagnostic purpose of the model operation. The
575 individual signals contribute to the global anomaly prediction, while the pro-
576 posed dynamic limits offer less conservative restrictions on individual process
577 operation. In parallel, the detector allows discrimination of signal losses due
578 to packet drops and sensor malfunctioning.

579 The ability to detect and identify anomalies in the system, isolate the
580 root cause of anomaly to specific signal or feature, and identify signal losses
581 is shown in two case studies on real data. Unlike many anomaly detec-
582 tion approaches, the proposed AID method does not require historical data
583 or ground truth information about anomalies, relieving general limitations.
584 Moreover, it combines adaptability and interpretability, which is an area yet
585 to be explored.

586 The benchmark performed on industrial data showed the ability to pro-
587 vide comparable results to other self-learning adaptable anomaly detection
588 methods. This is an important property for our model which allows, in
589 addition, the root cause isolation. The first case study, performed on real
590 operation data of BESS, examined the battery energy storage system and

591 demonstrated the ability to capture system anomalies and provide less con-
592 servative limits to signals. The physical model aided decisions about the
593 normality of the measured temperature of BESS.

594 The second case study exposed the ability to detect anomalies in the
595 temperature profiles of battery modules within the battery pack, considering
596 measurements made by multiple sensors distributed around the module and
597 the average temperature of all the modules within the pack. Hardware fault
598 observed on this deployed device was captured by our model, giving another
599 proof of its importance in energy storage systems monitoring, where tight
600 temperature control plays a significant role in the safety and profitability of
601 the system.

602 Future works on the method will include improvement to the change point
603 detection mechanism, decrease in the latency on high dimensional data, and
604 false positive rate reduction, from which general plug-and-play models suffer.

605 References

606 V. Chandola, A. Banerjee, V. Kumar, Anomaly detection: A survey, ACM
607 Comput. Surv. 41 (2009). URL: <https://doi.org/10.1145/1541880.1541882>. doi:10.1145/1541880.1541882.

609 N. Laptev, S. Amizadeh, I. Flint, Generic and scalable framework for auto-
610 mated time-series anomaly detection, in: Proceedings of the 21th ACM
611 SIGKDD International Conference on Knowledge Discovery and Data Min-
612 ing, KDD '15, Association for Computing Machinery, New York, NY,
613 USA, 2015, pp. 1939–1947. URL: <https://doi.org/10.1145/2783258.2788611>. doi:10.1145/2783258.2788611.

615 A. Kejariwal, Introducing practical and robust anomaly
616 detection in a time series, 2015. URL: https://blog.twitter.com/engineering/en_us/a/2015/introducing-practical-and-robust-anomaly-detection-in-a-time-series.

619 A. A. Cook, G. Misirli, Z. Fan, Anomaly detection for iot time-series data:
620 A survey, IEEE Internet of Things Journal 7 (2020) 6481–6494. doi:10.
621 1109/JIOT.2019.2958185.

622 C. Fan, Y. Sun, Y. Zhao, M. Song, J. Wang, Deep learning-based fea-
623 ture engineering methods for improved building energy prediction, Ap-
624 plied Energy 240 (2019) 35–45. URL: <https://www.sciencedirect.com>.

- 625 com/science/article/pii/S0306261919303496. doi:<https://doi.org/10.1016/j.apenergy.2019.02.052>.
- 626
- 627 P. D. Talagala, R. J. Hyndman, K. Smith-Miles, Anomaly detection
628 in high-dimensional data, Journal of Computational and Graphi-
629 cal Statistics 30 (2021) 360–374. URL: <https://doi.org/10.1080/10618600.2020.1807997>.
630 doi:10.1080/10618600.2020.1807997.
631 arXiv:<https://doi.org/10.1080/10618600.2020.1807997>.
- 632 M. Salehi, L. Rashidi, A survey on anomaly detection in evolving data:
633 [with application to forest fire risk prediction], SIGKDD Explor. Newsl.
634 20 (2018) 13–23. URL: <https://doi.org/10.1145/3229329.3229332>.
635 doi:10.1145/3229329.3229332.
- 636 N. Barbosa Roa, L. Travé-Massuyès, V. H. Grisales-Palacio, Dy-
637 clee: Dynamic clustering for tracking evolving environments, Pat-
638 tern Recognition 94 (2019) 162–186. URL: <https://www.sciencedirect.com/science/article/pii/S0031320319301992>. doi:<https://doi.org/10.1016/j.patcog.2019.05.024>.
- 639
- 640
- 641 A. G. Tartakovsky, A. S. Polunchenko, G. Sokolov, Efficient computer net-
642 work anomaly detection by changepoint detection methods, IEEE Journal
643 of Selected Topics in Signal Processing 7 (2013) 4–11. doi:10.1109/JSTSP.
644 2012.2233713.
- 645 H. Wu, J. He, M. Tömösközi, Z. Xiang, F. H. Fitzek, In-network processing
646 for low-latency industrial anomaly detection in softwarized networks, in:
647 2021 IEEE Global Communications Conference (GLOBECOM), 2021, pp.
648 01–07. doi:10.1109/GLOBECOM46510.2021.9685489.
- 649 H. S. Pannu, J. Liu, S. Fu, Aad: Adaptive anomaly detection system for cloud
650 computing infrastructures, in: 2012 IEEE 31st Symposium on Reliable
651 Distributed Systems, 2012, pp. 396–397. doi:10.1109/SRDS.2012.3.
- 652 S. Ahmad, A. Lavin, S. Purdy, Z. Agha, Unsupervised real-time anomaly
653 detection for streaming data, Neurocomputing 262 (2017) 134–
654 147. URL: <https://www.sciencedirect.com/science/article/pii/S0925231217309864>. doi:<https://doi.org/10.1016/j.neucom.2017.04.070>, online Real-Time Learning Strategies for Data Streams.
- 655
- 656

- 657 H. H. Bosman, G. Iacca, A. Tejada, H. J. Wörtche, A. Liotta, Ensembles
658 of incremental learners to detect anomalies in ad hoc sensor networks,
659 Ad Hoc Networks 35 (2015) 14–36. URL: <https://www.sciencedirect.com/science/article/pii/S1570870515001481>. doi:<https://doi.org/10.1016/j.adhoc.2015.07.013>, special Issue on Big Data Inspired Data
660 Sensing, Processing and Networking Technologies.
- 661
- 662
- 663 M. Carletti, C. Masiero, A. Beghi, G. A. Susto, Explainable machine learning
664 in industry 4.0: Evaluating feature importance in anomaly detection to
665 enable root cause analysis, in: 2019 IEEE International Conference on
666 Systems, Man and Cybernetics (SMC), 2019, pp. 21–26. doi:[10.1109/SMC.2019.8913901](https://doi.org/10.1109/SMC.2019.8913901).
- 667
- 668 Q. P. Nguyen, K. W. Lim, D. M. Divakaran, K. H. Low, M. C. Chan, Gee: A
669 gradient-based explainable variational autoencoder for network anomaly
670 detection, in: 2019 IEEE Conference on Communications and Network
671 Security (CNS), 2019, pp. 91–99. doi:[10.1109/CNS.2019.8802833](https://doi.org/10.1109/CNS.2019.8802833).
- 672
- 673 K. Amarasinghe, K. Kenney, M. Manic, Toward explainable deep neural
674 network based anomaly detection, in: 2018 11th International Conference
675 on Human System Interaction (HSI), 2018, pp. 311–317. doi:[10.1109/HSI.2018.8430788](https://doi.org/10.1109/HSI.2018.8430788).
- 676
- 677 W.-T. Yang, M. S. Reis, V. Borodin, M. Juge, A. Roussy, An interpretable
678 unsupervised bayesian network model for fault detection and diagno-
679 sis, Control Engineering Practice 127 (2022) 105304. URL: <https://www.sciencedirect.com/science/article/pii/S0967066122001502>.
680 doi:<https://doi.org/10.1016/j.conengprac.2022.105304>.
- 681
- 682 M. Wadinger, M. Kvasnica, Real-time outlier detection with dynamic pro-
683 cess limits, in: Proceedings of the 2023 24th International Conference on
Process Control (PC), 2023. In press.
- 684
- 685 K. Yamanishi, J.-i. Takeuchi, A unifying framework for detecting outliers and
686 change points from non-stationary time series data, in: Proceedings of the
687 Eighth ACM SIGKDD International Conference on Knowledge Discovery
688 and Data Mining, KDD '02, Association for Computing Machinery, New
689 York, NY, USA, 2002, pp. 676–681. URL: <https://doi.org/10.1145/775047.775148>. doi:[10.1145/775047.775148](https://doi.org/10.1145/775047.775148).
- 689

- 690 K. Yamanishi, J.-i. Takeuchi, G. Williams, P. Milne, On-line unsu-
691 pervised outlier detection using finite mixtures with discounting learn-
692 ing algorithms, Data Mining and Knowledge Discovery 8 (2004) 275–
693 300. URL: <https://doi.org/10.1023/B:DAMI.0000023676.72185.7c>.
694 doi:10.1023/B:DAMI.0000023676.72185.7c.
- 695 B. Steenwinckel, Adaptive anomaly detection and root cause analysis by fus-
696 ing semantics and machine learning, in: A. Gangemi, A. L. Gentile, A. G.
697 Nuzzolese, S. Rudolph, M. Maleshkova, H. Paulheim, J. Z. Pan, M. Alam
698 (Eds.), The Semantic Web: ESWC 2018 Satellite Events, Springer Inter-
699 national Publishing, Cham, 2018, pp. 272–282.
- 700 B. Steenwinckel, D. De Paepe, S. Vanden Hautte, P. Heyvaert, M. Ben-
701 tefrit, P. Moens, A. Dimou, B. Van Den Bossche, F. De Turck, S. Van
702 Hoecke, F. Ongena, Flags: A methodology for adaptive anomaly
703 detection and root cause analysis on sensor data streams by fusing
704 expert knowledge with machine learning, Future Generation Com-
705 puter Systems 116 (2021) 30–48. URL: <https://www.sciencedirect.com/science/article/pii/S0167739X20329927>. doi:<https://doi.org/10.1016/j.future.2020.10.015>.
- 706 707
- 708 M. Amer, M. Goldstein, S. Abdennadher, Enhancing one-class support vec-
709 tor machines for unsupervised anomaly detection, in: Proceedings of the
710 ACM SIGKDD Workshop on Outlier Detection and Description, ODD ’13,
711 Association for Computing Machinery, New York, NY, USA, 2013, pp.
712 8–15. URL: <https://doi.org/10.1145/2500853.2500857>.
713 doi:10.1145/2500853.2500857.
- 714 B. Liu, Y. Xiao, P. S. Yu, L. Cao, Y. Zhang, Z. Hao, Uncertain one-class
715 learning and concept summarization learning on uncertain data streams,
716 IEEE Transactions on Knowledge and Data Engineering 26 (2014) 468–
717 484. doi:10.1109/TKDE.2012.235.
- 718 B. Krawczyk, M. Woźniak, One-class classifiers with incremental
719 learning and forgetting for data streams with concept drift, Soft
720 Computing 19 (2015) 3387–3400. URL: <https://doi.org/10.1007/s00500-014-1492-5>.
721 doi:10.1007/s00500-014-1492-5.
- 722 X. Miao, Y. Liu, H. Zhao, C. Li, Distributed online one-class support vec-

- 723 tor machine for anomaly detection over networks, IEEE Transactions on
724 Cybernetics 49 (2019) 1475–1488. doi:10.1109/TCYB.2018.2804940.
- 725 Ö. Gözüaçık, F. Can, Concept learning using one-class classifiers for
726 implicit drift detection in evolving data streams, Artificial Intelligence
727 Review 54 (2021) 3725–3747. URL: <https://doi.org/10.1007/s10462-020-09939-x>. doi:10.1007/s10462-020-09939-x.
- 729 R. Wetzig, A. Gulenko, F. Schmidt, Unsupervised anomaly alerting for
730 iot-gateway monitoring using adaptive thresholds and half-space trees,
731 in: 2019 Sixth International Conference on Internet of Things: Systems,
732 Management and Security (IOTSMS), 2019, pp. 161–168. doi:10.1109/IOTSMS48152.2019.8939201.
- 734 Y. Lyu, W. Li, Y. Wang, S. Sun, C. Wang, Rmhsforest: Rel-
735 ative mass and half-space tree based forest for anomaly detec-
736 tion, Chinese Journal of Electronics 29 (2020) 1093–1101. URL:
737 <https://ietresearch.onlinelibrary.wiley.com/doi/abs/10.1049/cje.2020.09.010>.
738 doi:<https://doi.org/10.1049/cje.2020.09.010>.
739 arXiv:<https://ietresearch.onlinelibrary.wiley.com/doi/pdf/10.1049/cje.2020.09.010>
- 740 B. P. Welford, Note on a method for calculating corrected
741 sums of squares and products, Technometrics 4 (1962) 419–
742 420. URL: <https://www.tandfonline.com/doi/abs/10.1080/00401706.1962.10490022>.
743 doi:10.1080/00401706.1962.10490022.
744 arXiv:<https://www.tandfonline.com/doi/pdf/10.1080/00401706.1962.10490022>.
- 745 A. Genz, Numerical computation of multivariate normal probabilities, Jour-
746 nal of Computational and Graphical Statistics 1 (2000). doi:10.1080/
747 10618600.1992.10477010.
- 748 R. P. Brent, Algorithms for minimization without derivatives, Prentice-Hall,
749 Englewood Cliffs, N.J, 1972. URL: https://openlibrary.org/books/OL4739237M/Algorithms_for_minimization_without_derivatives.
- 751 F. Iglesias Vázquez, A. Hartl, T. Zseby, A. Zimek, Anomaly detection in
752 streaming data: A comparison and evaluation study, Expert Systems with
753 Applications 233 (2023) 120994. URL: <https://www.sciencedirect.com/science/article/pii/S0957417423014963>. doi:<https://doi.org/10.1016/j.eswa.2023.120994>.

756 L. Ruff, J. R. Kauffmann, R. A. Vandermeulen, G. Montavon, W. Samek,
757 M. Kloft, T. G. Dietterich, K.-R. Müller, A unifying review of deep and
758 shallow anomaly detection, *Proceedings of the IEEE* 109 (2021) 756–795.
759 doi:10.1109/JPROC.2021.3052449.

760 I. D. Katser, V. O. Kozitsin, Skoltech anomaly benchmark (skab),
761 <https://www.kaggle.com/dsv/1693952>, 2020. doi:10.34740/KAGGLE/
762 DSV/1693952.